Proceedings of the Royal Society A 470 (2014) 20140108

Hydrogen diffusion and the percolation of austenite in nanostructured bainitic steel

AUTHORS:
Lucy Fielding [a] (corresponding author)
Eun Ju Song [b]
Do-Kyeong Han [b]
Harshad Bhadeshia [a,b]
Dong-Woo Suh [b]

[a] Department of Materials Science and Metallurgy
University of Cambridge
United Kingdom

[b] Graduate Institute of Ferrous Technology
POSTECH
Republic of Korea

Contact details for corresponding author:
Postal address:
Department of Materials Science and Metallurgy
University of Cambridge
27 Charles Babbage Road
Cambridge
CB3 0FS
Email: lcdf2@cam.ac.uk
Phone: +441223 334 336

Proceedings of the Royal Society A 470 (2014) 20140108

Hydrogen diffusion and the percolation of austenite in nanostructured bainitic steel

L. C. D. Fielding[a], E. J. Song[b], D. K. Han[b], H. K. D. H. Bhadeshia[a,b], D.-W. Suh[b]

[a]*Materials Science and Metallurgy, University of Cambridge, U.K*

[b]*Graduate Institute of Ferrous Technology, POSTECH, Republic of Korea*

Abstract

The diffusion of hydrogen in austenite is slower than in ferrite. Experiments have been conducted to study the behaviour of hydrogen in a nanostructured steel sample consisting of a mixture of thin plates of bainitic ferrite and intervening films of retained austenite, with the latter phase present in a quantity larger than the percolation threshold, i.e, it has three-dimensional connectivity. The structure was then heat treated to control the fraction of austenite, and hence to study the role of hydrogen when the austenite decomposes below the value required to sustain percolation. The experiments have involved both thermal desorption analysis and permeation, and when combined with theoretical analysis, indicate a significant influence of percolating austenite in hindering the passage of hydrogen into the steel during hydrogen charging, and its permeation through the composite nanostructure. The effect is not as large as might be expected from a simple comparison of independent data on the diffusivities of hydrogen in the two lattices, because the effective diffusivity in ferrite is found to be much smaller than in the defect-free ferrite, due to trapping effects. The morphology of the austenite is demonstrated to play a role by comparing with a sample containing a larger volume fraction of austenite but present as isolated grains which are ineffective to the permeation of hydrogen.

Keywords: Bainitic steels; Nanostructured metals; Hydrogen desorption; Gas permeability; Austenite percolation

1. Introduction

Nanostructured bainite consists of exceptionally thin platelets of bainitic ferrite separated by films of retained austenite, a structure produced by heat treatment alone [1–3], and yet resulting in an interfacial area per unit volume that is greater than that associated with the majority of severe plastic deformation experiments [4]. The tensile behaviour is characterised by uniform elongation accompanied by little, if any necking [5–7]. The uniform elongation therefore is usually equal to the total elongation. In general, tensile tests reveal a dependence of ductility upon transformation temperature, and an inverse correlation with strength [6, 8]. In carbide-free bainitic steels, such as superbainite, the volume fraction and morphology of austenite are controlling factors in the ductility [9, 10]. In particular, the TRIP[1] effect comes into play – retained austenite transforms into martensite under tensile loading. This process is influenced by various factors relating to austenite stability, such as grain orientation, morphology, carbon content and scale [7, 11–15].

2. Motivation

It is possible to use standard calculation methods [16–18] to follow the variation in retained austenite during tensile tests on nanostructured bainite as a function of plastic strain, accounting for austenite composition and the temperature at which deformation occurs. It then becomes evident that the strain at the point of fracture consistently occurs when the austenite volume fraction is reduced to about 0.1, a conclusion supported by *in situ* tests in which phase fractions are monitored during tensile testing [15]. It has therefore been argued that in these steels, the failure in tension occurs when the retained austenite loses three-dimensional [19]. This means that regions of austenite become geometrically isolated from one another, to the extent that it is no longer possible for applied stresses and strains to 'trace a path' that passes only through the austenite phase. At this point, the stresses must additionally be borne by the more brittle martensite that results from the deformation-induced transformation of austenite, leading to fracture. Measurements of austenite volume fraction at various locations in tested tensile specimens support this idea [7]. The need to control the mechanical stability

[1] Transformation-induced plasticity.

of retained austenite in automotive TRIP-assisted steels in order to ensure an optimised uniform ductility has long been recognised [20], but the important difference here is that with bulk nanostructured bainitic steel, the ductility is essentially all uniform and a different mechanism seems to govern ultimate fracture.

Our goal in the present work was to use thermal desorption analysis (TDA) techniques on hydrogen-charged samples to test the hypothesis that the austenite in a nanostructured steel loses percolation at a volume fraction of about 0.1. A great deal of peripheral information on the distribution of hydrogen in the two-phase ferrite plus austenite mixture is obtained at the same time. The logic of the experiments is based on the fact that the diffusivity and solubility of hydrogen is dramatically different in the two phases, with diffusion being much slower in austenite. It follows that in a percolating structure, less hydrogen should be able to penetrate the sample for a given charging time, because the hydrogen must necessarily diffuse through austenite at some stage.

3. Experimental Methods

Thermal desorption analysis is a technique normally used to study hydrogen trapping states [21, 22]. Specimens are charged electrolytically with hydrogen and then heated at a constant rate, with any desorbed hydrogen detected using gas chromatography. Strongly trapped hydrogen is released at a higher temperature, and the total released can be detected by integrating the data over the time period of the experiment.

The chemical composition of the steels used in this experiment are given in Table 1. The vast majority of experiments reported here have been conducted on Alloy 1, but because of the limited material available, some of the experiments are on Alloy 2. Both can be heat-treated to produce the required nanostructure, as shown previously [1, 2, 23, 24]. Alloy 1 was austenitised in an argon tube furnace at 900°C for 30 min, followed by isothermal transformation at 200°C for 96 h. Specimens measuring 55 mm × 12 mm × 4 mm were produced from the isothermally transformed sample of Alloy 1.

Alloy 2 was similarly austenitised at 850°C for 1 h and then isothermally transformed at 200°C for 168 h, a longer period than Alloy 1, because it does not contain the Co or Al that accelerates transformation [24]. The

Alloy	C	Si	Mn	Mo	Cr	Co	Al	Ni	P	S
Alloy 1	0.79	1.56	1.98	0.24	1.01	1.51	1.01	–	0.002	0.002
Alloy 2	0.80	1.51	2.03	0.38	0.22	–	0.57	1.05	0.006	0.006
Alloy 3	0.11	–	6.17	–	–	–	0.98	–	–	–

Table 1: Chemical compositions, wt%. Alloys 1 and 2 represent the nanostructured bainite, whereas Alloy 3 is a much coarser mixture of austenite and ferrite.

samples were in this case produced as 55 mm × 20 mm × 1 mm size because they were destined primarily for permeation experiments, and to establish the saturation concentrations of hydrogen.

In order to vary the volume fraction of austenite, the isothermally transformed samples were tempered to various extents as detailed in Table 2. The austenite volume fraction (V_γ) was measured using quantitative X-ray analysis. After tempering, the samples were ground with progressively finer grades of silicon carbide paper, up to 4000 grit. They were then etched to remove deformed layers generated while grinding. X-ray work was carried out by step-scanning on a Philips PW150 X-ray diffractometer using unfiltered Cu K_α radiation, operated at 40 kV and 40 mA. The 2θ scanning speed was $0.1^\circ\,\mathrm{min}^{-1}$ over a range of 40-140°. Rietveld refinement was done using Panalytic HighScore Plus software, and retained austenite carbon content was calculated from the measured lattice parameters as described by Dyson and Holmes [25].

The samples were polished with 220-grit and 800-grit silicon carbide papers, cleaned with high-purity ethanol and electrochemically charged with hydrogen in an aqueous mixture of 3% NaCl + 0.3% NH_4SCN, using a current density of $1\,\mathrm{A\,m}^{-2}$. The standard charging time used was 24 h, although this was varied from 1-6 h in the later stages of the experiment, in order to study the effect of charging time.

Figure 1a shows a schematic diagram of the TDA set-up. After charging, each sample was cleaned with ethanol, dried and placed in the furnace tube. The time interval between the completion of charging and placing the sample in the furnace was 5 min. Samples were heated to 700°C at a rate of $100^\circ\mathrm{C\,h}^{-1}$. The sample gas was analysed at 3-minute intervals using helium as a carrier gas. This transfers the desorbed hydrogen into the gas

Alloy	Tempering temperature / °C	Tempering time / h	V_γ
1	Untempered	–	0.21
1	450	2.0	0.15
1	500	0.5	0.10
1	500	1.0	0.07
2	Untempered	–	0.15
2	450	2.0	0.07
2	500	0.5	0.03
2	500	1.0	0.02
3	620	24.0	0.26

Table 2: List of tempering heat-treatments used, and the retained austenite content of each sample. In the case of Alloy 3, the actual mixture of austenite and ferrite is generated by annealing at the designated temperature.

chromatograph where it is monitored by a detector. The hydrogen content was calibrated using a standard gas mixture. In the TDA results presented here, the quantity of hydrogen desorbed is expressed in units of ppmw, representing the parts per million by weight of hydrogen relative to the sample weight.

The electrochemical hydrogen permeation cell used to measure the effective diffusivity of hydrogen through the variety of structures is illustrated in Fig. 1b. The test was performed according to the ISO17081 standard. The detailed procedure is described elsewhere [26] but the test permits, in particular, the effective diffusivity and permeability to be determined by monitoring the current density through the sample as a function of time. The steady state flux of hydrogen through the sample is $J_{ss} = i_{ss}/n\mathrm{F}$ where i_{ss} is the steady state current density, F is the Faraday constant, and n the number of electrons that participate in the electrochemical reaction. The permeability is then simply $J_{ss}L$, where L is the sample thickness. A time lag t_l is defined to be that required to achieve 0.63 of the steady-state current density, and the effective diffusivity as calculated from this time lag is simply $D_l = L^2/6t_l$. Alternatively, both the effective diffusivity and permeability may be calculated using the break-through method, in which the time t_b is defined as that at which the current density begins to increase after beginning the experiment. The effective diffusivity calculated in this way is $D_b = L^2/15.3t_b$.

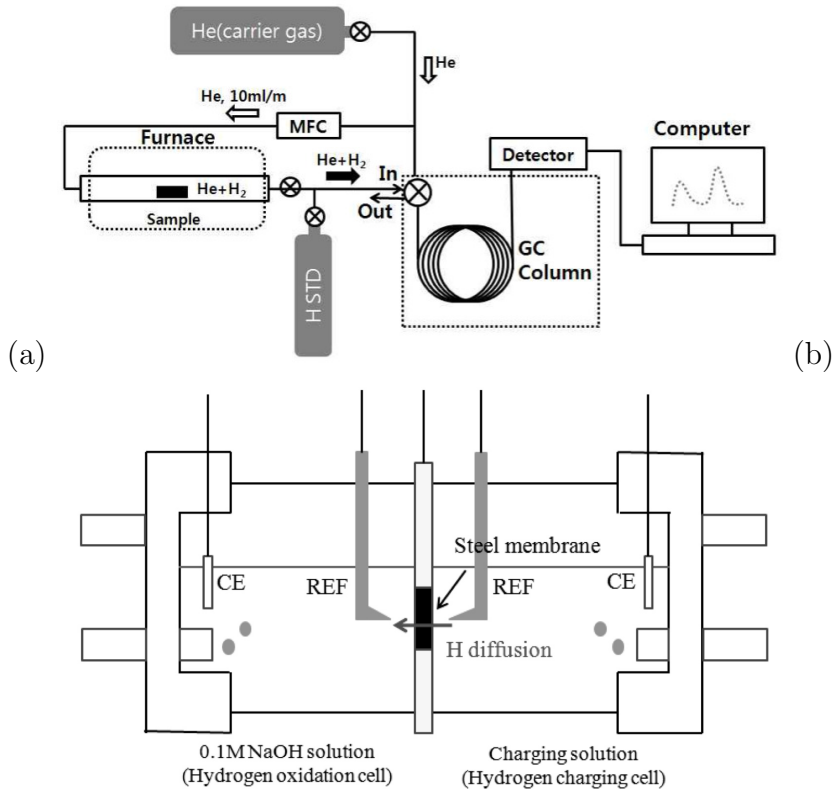

Figure 1: Schematic diagrams showing (a) thermal desorption and (b) Devanathan-Stachurski permeation cell used.

Transmission electron microscopy was carried out on a JEOL 200CX microscope. Samples were prepared by slicing thin sections from heat-treated specimens and grinding them with 340-grade silicon carbide papers until the thickness reached 70 μm. Circular samples 3 mm in diameter were punched out from these sections and ground down with 2500-grade silicon carbide papers until the thickness reached 50 μm. These samples were electropolished at 20 V in a twin jet unit with a 15 vol% perchloric acid-85 vol% ethanol electrolyte.

Vickers hardness testing was carried out at a load of 30 kg. Samples were cut from the tempered specimens and mounted in resin. They were polished to a mirror finish with 600-grade, 800-grade, 2500-grade and 4000-grade silicon carbide papers. Eight hardness measurements were taken from each sample, and averaged.

4. Results and Discussion

4.1. TEM Characterisation

Tempering treatment	Final V_γ	Austenite carbon content/wt%	Hardness/HV30
Alloy 1			
Untempered	0.21	1.21±0.01	616±2
400°C for 1 h	0.19		
400°C for 2 h	0.18		
450°C for 1 h	0.18		
450°C for 2 h	0.15	0.97±0.01	588±2
500°C for 30 min	0.10	0.78±0.03	571±1
500°C for 1 h	0.07	0.75±0.03	569±2
Alloy 2			
Untempered	0.15		626±7
450°C for 2 h	0.07		606±7
500°C for 30 min	0.03		579±8
500°C for 1 h	0.02		550±4

Table 3: Hardness values for each set of samples. The retained austenite content has, in each case, an uncertainty in volume fraction of about ±0.01.

Both of the nanostructured alloys were characterised using transmission electron micrography and hardness testing. Much more detailed structural char-

acterisation has been reported elsewhere [3, 15, 27] and so is not repeated here. The as-transformed structure of Alloy 1 is shown in Figure 2a. The alloy initially consists of two phases: bainitic ferrite and retained austenite, both of which are visible as thin plates and films in Figure 2a. Previous work has found that the bainite plate thickness in this alloy ranges from 12-45 nm when transformed at 200°C [3, 15]. The structure also contains some regions of fine blocky-austenite; the reported ratio of film-austenite to blocky-austenite in this alloy, when transformed at 200°C, is approximately 3:1 by volume [3]. The as-transformed structure of Alloy 2, shown in Figure 3a, is coarser, with an average plate thickness of 83± nm.

Bainitic steels, such as the alloys studied here, are resistant to tempering, with little reduction in hardness or austenite volume fraction below 450°C and significant softening only taking place at temperatures above 500°C [27–29]. This is reflected in the fact that the hardness remains high in both alloys, even after tempering at 500°C for one hour. However, the reduction in hardness following the tempering treatments signals the onset of austenite decomposition, as confirmed by X-ray analysis (Table 3). Attempts to temper Alloy 1 at temperatures below 450°C did not produce a particularly significant change in austenite volume fraction. Therefore, no such treatments were applied to Alloy 2.

Tempering that leads to carbide precipitation from the decomposition of austenite, also hinders the coarsening of the ferrite plates since the carbides in fact are located precisely at the plate boundaries, thus preventing significant coarsening [27]. Therefore, the plate structure is preserved after all the tempering heat treatments, as illustrated in Figs. 2 and 3. All the tempering treatments listed in Table 3 led to carbide precipitation in Alloy 1 (Fig. 2b-d). The carbides were confirmed to be cementite using electron diffraction (Fig. 4); note that the as-transformed material is carbide-free because of the large silicon concentration in the steel. Cementite was also detected in Alloy 2 after all tempering treatments at 500°C (Fig. 3d; Fig. 4c, d). Although no carbides were found after tempering Alloy 2 at 450°C, it is possible that the volume fraction of any carbides is smaller than can be easily detected.

A topologically different kind of a mixture of ferrite and austenite, where the latter is distributed as non-percolating grains was generated in a dual-phase steel of composition Fe-0.11C-6.17Mn-0.98Al wt%, by isothermal heat treatment at 620°C for 24 h, as illustrated in Fig. 5. This alloy is interesting

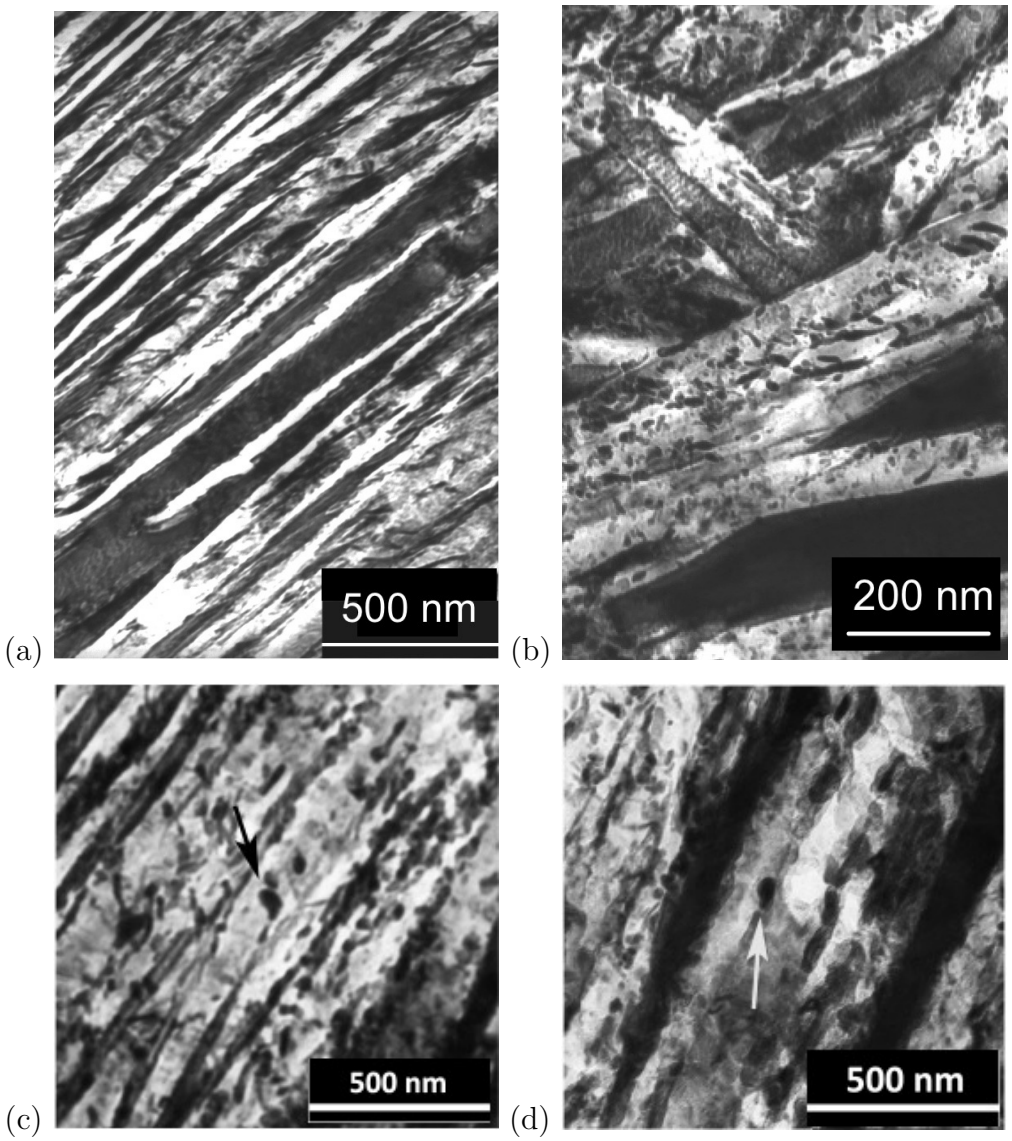

Figure 2: Alloy 1. (a) As-transformed structure, with the darker regions representing retained austenite. (b) Structure containing some carbide particles, after tempering 450°C for 2 h. (c) After tempering 500°C for 0.5 h. (d) After tempering 500°C for 1 h. Carbide particles are arrowed.

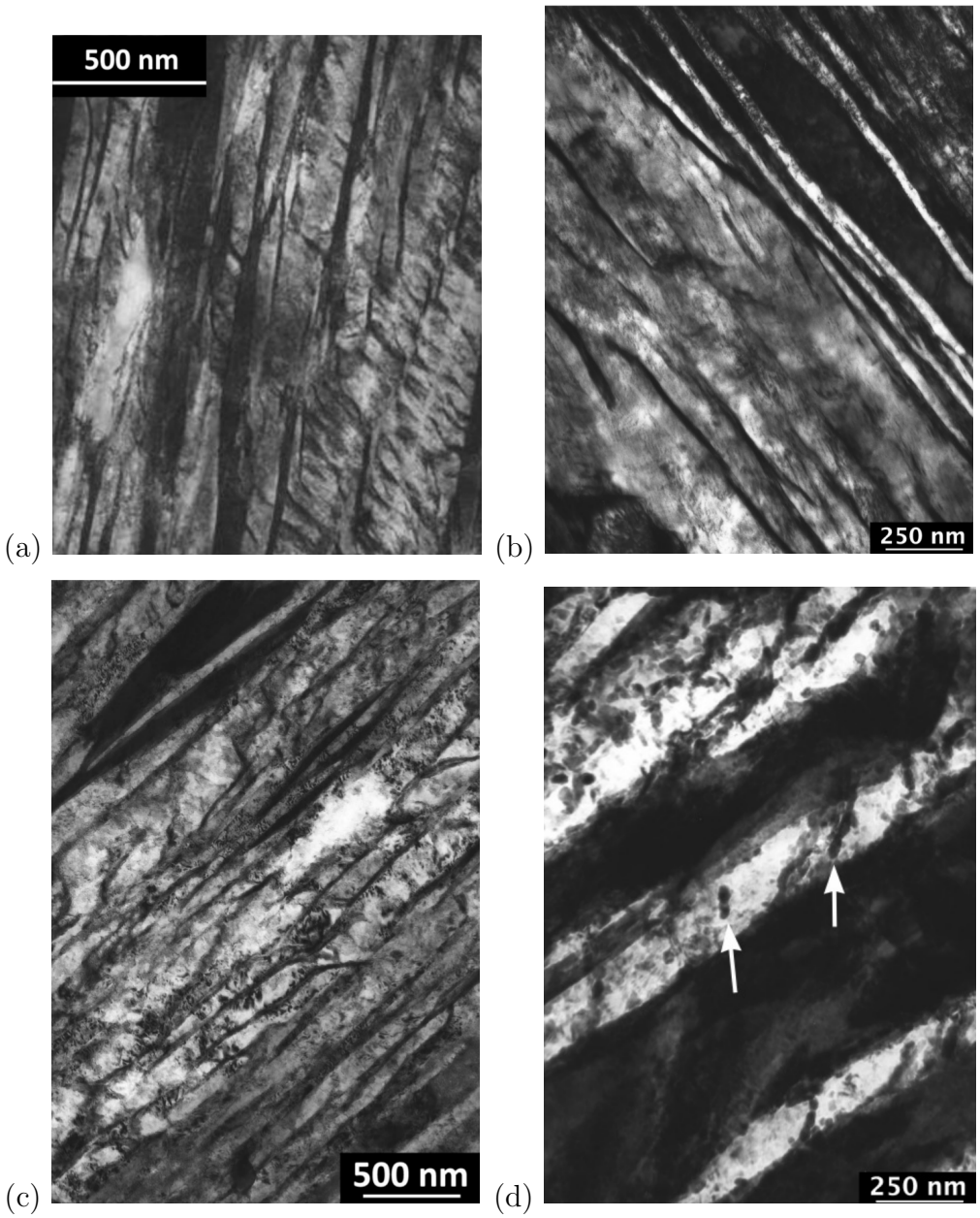

Figure 3: Alloy 2. (a) As-transformed structure, with the darker regions representing retained austenite. (b) After tempering 450°C for 2 h. (c) After tempering 500°C for 0.5 h. (d) After tempering 500°C for 1 h. Carbide particles are arrowed.

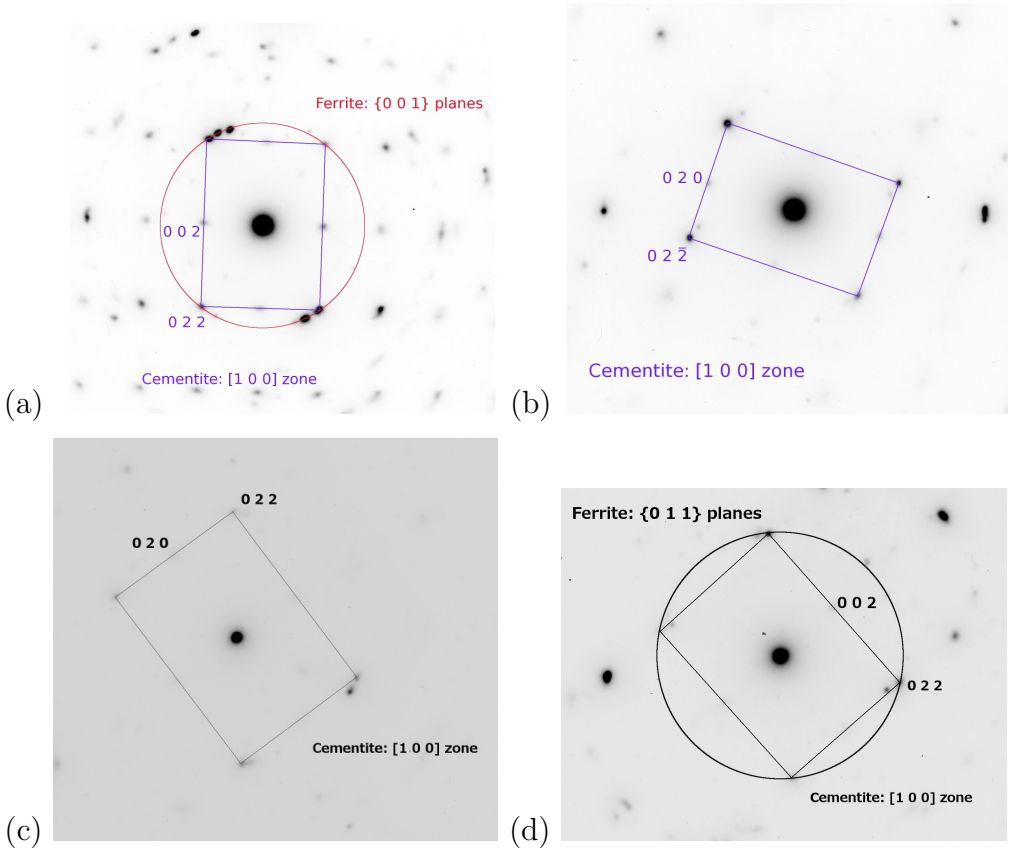

Figure 4: Electron diffraction patterns confirming the presence of cementite. (a) Alloy 1, after tempering at 450°C for 2 h. (b) Alloy 1, after tempering at 500°C for 1 h. (c) Alloy 2, after tempering at 500°C for 30 min. (d) Alloy 2, after tempering at 500°C for 1 h.

because the morphology is such that austenite grains are isolated, with continuity for any hydrogen to permeate through the ferrite where the hydrogen is much more mobile.

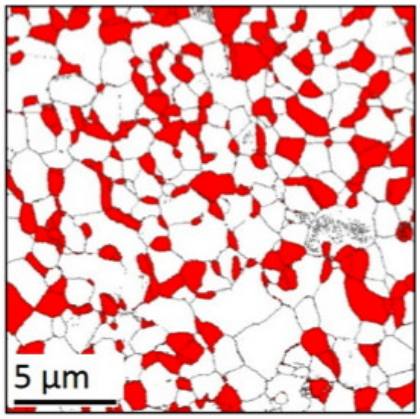

Figure 5: Alloy 3. EBSD phase map with red and white regions indicating austenite ($V_\gamma = 0.26$) and ferrite respectively.

4.2. Thermal Desorption Analysis

There are two essential categories of hydrogen in steel: that which is diffusible and can in principle escape from the steel, and the remainder, which is said to be trapped and is much more difficult to remove. The concept of hydrogen-trapping comes from Darken and Smith [30] who established that the passage of hydrogen through a steel is hindered by lattice imperfections (dislocations, interfaces) that tend to attract and bind it, thus rendering it immobile at temperatures where it should diffuse readily. The binding energy is defect dependent [31]. In two-phase mixtures of austenite and ferrite, of the type relevant to the present studies, the diffusivity of hydrogen in perfect austenite is far smaller than in ferrite, although its solubility in austenite is much greater than in ferrite. The austenite can, in this sense, be regarded as a macroscopic trap for hydrogen, relative to the ease with which hydrogen can diffuse in ferrite [32]. Therefore, in a thermal desorption experiment, the hydrogen in austenite is expected to be detected at a higher temperature during heating than that from ferrite, which may be released at close to ambient temperature.

Given the complexity of the problem, several experiments were carried out to understand the response of the hydrogen-charged and uncharged samples

when subjected to thermal desorption analysis; these are reported first, before a discussion of the main results.

4.3. "Calibration" experiments

A sample of Alloy 1 was subjected to TDA before deliberate charging with hydrogen. Fig. 6a shows the TDA output from an uncharged untempered sample with $V_\gamma = 0.21$, heated at $100°C\,min^{-1}$. The little hydrogen evolved does so at temperatures below 50°C, which means that it is not dissolved in the steel since it is easily desorbed. The origin of this low-temperature evolution is not clear, but the quantity desorbed between room temperature and 300°C amounts to just 0.17 ppmw and can be neglected.

Fig. 6b details the experiments done to assess the reproducibility of data from physically distinct samples that have been identically heat-treated and charged. The variability is likely to be due to specimen rather than instrument scatter, since the structures involved are complex.

A significant goal of the present work was to see whether the films of austenite present in the nanostructure impede the motion of hydrogen by percolating through the structure. Clearly, in order to assess this, the structure must not be saturated with hydrogen prior to the thermal desorption analysis. At the same time, sufficient hydrogen must be charged to ensure a good signal-to-noise ratio. The samples of Alloy 1 were therefore made 4 mm in thickness, so as to allow sufficient hydrogen to enter the specimen surface, but leaving the core with a reduced concentration. Both samples were charged using the same current density. In this way, the amount of hydrogen that effuses during TDA is a reflection of its permeation into the sample. Fig. 6 compares the thickness effect for two samples, both transformed into nanostructured bainite at 200°C, albeit from slightly different alloys. The change in charging time from 24 h to 72 h did not alter the hydrogen content of the 1 mm thick sample, proving saturation. The total hydrogen desorbed 1 mm thick sample was measured to be 11.1 ppm, whereas that for the 4 mm thick sample was 19.6 ppm. The latter value should be much larger (at least 67 ppm given that the 4 mm sample is six times heavier) to match the saturation level of the thinner sample. The higher hydrogen content of the 4 mm sample indicates a somewhat greater penetration depth, since the penetration in the thinner sample cannot exceed 0.5 mm.

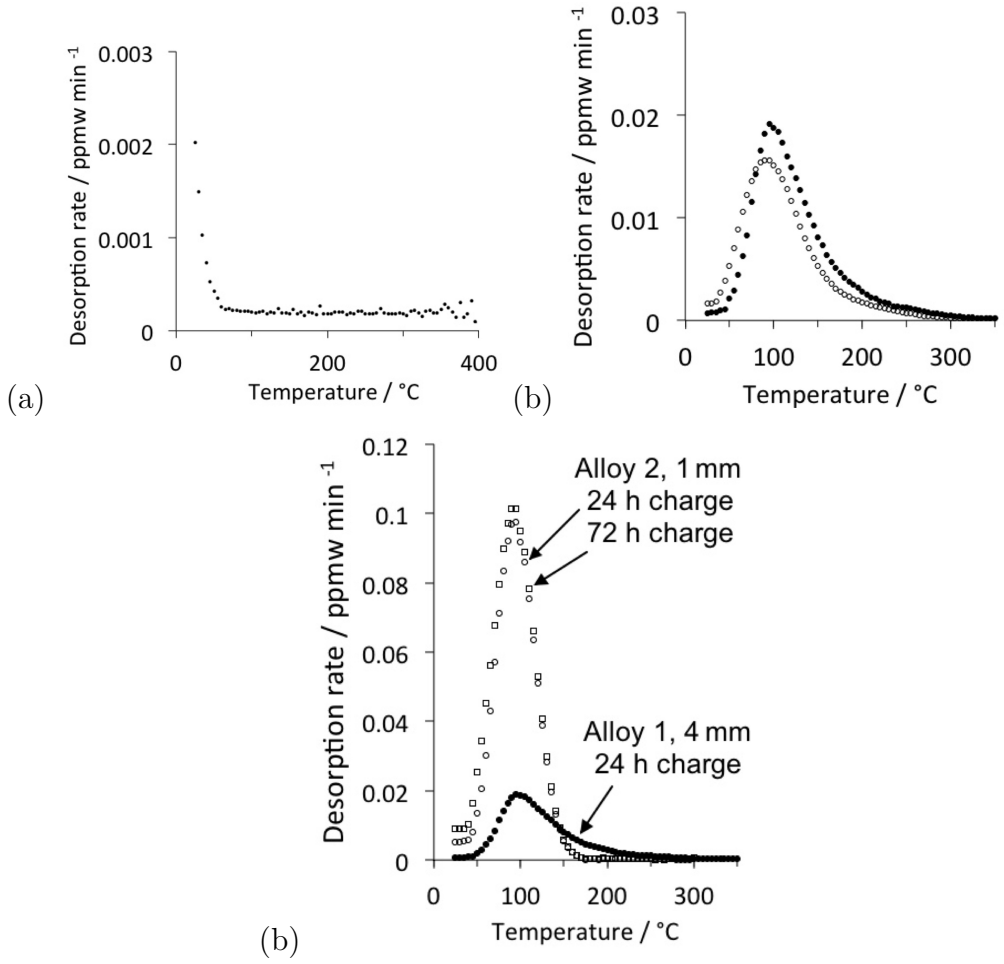

Figure 6: Thermal desorption analysis experiments at $100^{\circ}\mathrm{C\,h^{-1}}$, $V_\gamma = 0.21$. (a) Alloy 1, behaviour of an uncharged specimen. (b) Alloy 1, samples charged with hydrogen for 20 h. The two curves are from two physically different samples, identically produced before the TDA. (c) Comparison between TDA curves of 4 mm thick Alloy 1 samples, and 1 mm thick Alloy 2 sample.

4.4. Role of retained austenite

We first note that heating at the rates considered here, to temperatures up to 300°C, is sufficient to detrap hydrogen that is dissolved in austenite, and that from defects such as dislocations and interfaces. Such hydrogen is said to be reversibly trapped and is of particular interest in embrittlement phenomena.

TDA experiments were conducted on all the samples described in Table 3, after charging with hydrogen for 24 h, at 100°C min^{-1}. In Fig. 7, the three samples that contain $V_\gamma > 0.1$ show essentially similar behaviour; the two samples tested with $V_\gamma = 0.07$ show different behaviour, with one curve replicating the larger austenite data and the other consistent with a larger quantity of hydrogen penetrated into the sample during the charging process. It follows that these data alone cannot reveal differences due to the austenite content nor phenomena associated with the percolation threshold.

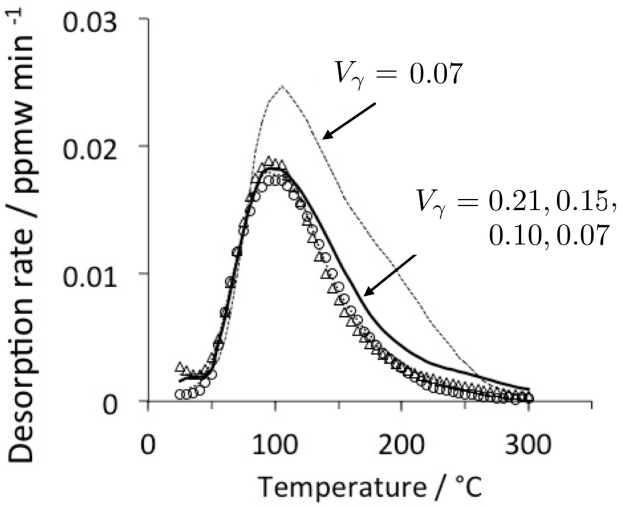

Figure 7: Alloy 1. TDA data collected after charging each of specimen with hydrogen for 24 h, using a heating rate of 100°C min^{-1}. The continuous line, triangles and circles correspond to $V_\gamma = 0.21$, 0.15, 0.10 of retained austenite. The dashed curves are for $V_\gamma = 0.07$, although one of these is not easily distinguished on the diagram, but lies between the triangles and circles.

Many further experiments were conducted to verify the general impression regarding the influence of retained austenite; the data are summarised in Table 4. It should be noted that the amount of hydrogen desorbed during heating over an appropriate temperature range is a reflection of the amount charged into the sample, as long as saturation does not set in.

Fig. 8a shows that the amount of hydrogen desorbed from the sample over the range 25-300°C, as expected, increases with the charging time. The re-

tained austenite content has minimal influence in the early stages of charging, presumably because there is sufficient exposed ferrite at the sample surface, of the 4 mm thick specimens. However, further penetration during charging is clearly more difficult for the sample with $V_\gamma = 0.21$ because the percolating austenite is a barrier to the diffusion of hydrogen in the sample.

Retained austenite should be a hindrance to the diffusion of hydrogen in a two-phase structure, and more so if its fraction is above a percolation threshold since there would then be no easy-diffusion paths. The data plotted in Fig. 8b as a function of retained austenite could be argued to further support the estimate [8] that austenite loses percolation in the bainitic sample when $V_\gamma \lesssim 0.1$. The desorbed hydrogen content (a reflection of the hydrogen that managed to enter the specimen) is clearly large when the percolation is lost.

However, this conclusion is not entirely established. It is not known whether there should be an abrupt change in hydrogen penetration into the sample when the percolation of austenite is lost, or whether the change should be gradual. A simple approach to this problem is illustrated in Fig. 9, where three scenarios are illustrated.[2] The first is the case where percolating film-like austenite dominates the movement of hydrogen, the second where both ferrite and austenite are exposed directly to the hydrogen and the third where the austenite films have been reduced to a fraction below the percolation threshold. Consider first the non-percolating structure (Fig. 9b) where both γ and α are exposed to the free surface. The net flux J_{os} per unit area into the 'open structure' is then

$$\begin{aligned} J_{os} &= AJ_\alpha + (1-A)J_\gamma \\ &\equiv J_\alpha\left[\frac{1}{\phi} + A\left(1 - \frac{1}{\phi}\right)\right] \end{aligned} \tag{1}$$

where A is the fraction of the free surface occupied by ferrite, $\phi = J_\alpha/J_\gamma$. In contrast, the flux J_p through the structure illustrated in Fig. 9a, where

[2]The model presented here is somewhat simplistic but it nevertheless captures the essence of the problem. A proper treatment that includes multiple phases, multiple traps and accounts for the morphology of the phases will require a numerical approach. A start has been made on the multiple trap problem for a single phase material [33] and attempts are now underway to to treat by numerical analysis, the more general problem that incorporates morphology.

the austenite in effect is a significant barrier to the infusion of hydrogen, is simply J_γ, which will vary inversely with the thickness t of the austenite film because that determines the magnitude of the concentration gradient given fixed boundary conditions. The thickness is here assumed to be proportional to the volume fraction of V_γ of austenite as long as the latter is above the percolation threshold:

$$J_p = J_\gamma/t \approx J_\gamma/V_\gamma. \qquad \text{for} \qquad V_\gamma > \text{percolation threshold} \tag{2}$$

The situation illustrated in Fig. 9c is where fraction of the film of austenite at the surface is less than unity, i.e., because the total fraction of austenite is less than the percolation threshold. For that case, the flux J_{np} is given by:

$$J_{np} = (1 - A)J_p + AJ_\alpha \qquad \text{for} \qquad V_\gamma < \text{percolation threshold} \tag{3}$$

The fluxes naturally depend on diffusion coefficients, and if it is assumed that undeformed ferrite and austenite have the diffusivities at 300 K of $D_\alpha = 1.26 \times 10^{-8}\,\mathrm{m^2\,s^{-1}}$ [31] and $D_\gamma = 2.65 \times 10^{-16}\,\mathrm{m^2\,s^{-1}}$ [34], then $J_\alpha \gg J_\gamma$ and there should be an overwhelming increase in the net flux as soon as percolation is lost. This does not in fact happen (Fig. 8). The reason is that the austenite-free structure obtained by tempering the mixture of bainitic ferrite and austenite still has a fine structure with dislocation and interface traps (the cementite itself is not a prominent trap in tempered structures [35]). Therefore, the appropriate D_α is that measured using permeation experiments on this structure, reported later in this paper to be $D_\alpha = 10^{-11}\,\mathrm{m^2\,s^{-1}}$; note also that this value is consistent with assessed data [36, Fig. 12]. The gradient of concentration is also determined by the solubility of hydrogen in the phase as a result of charging, the atom fractions taken to be $x_\alpha = 2.8 \times 10^{-8}$ and $x_\gamma = 7.0 \times 10^{-5}$ [37]. Using these values, the ratio $\phi = 15$ so equations 1 and 3 were used to calculate the variation in net flux as a function of the retained austenite content assuming $\phi = 15$ when $V_\gamma = 0.21$, the largest volume fraction of austenite in the bainitic samples.

Fig. 10 shows the results, where for the case with $V_\gamma = 0.07$, the area fraction A exposed to ferrite was taken to be 0.3, on the basis that no ferrite is exposed when $V_\gamma = 0.1$ since this is at the percolation threshold. It is evident that although there will be a significant change in the passage of the hydrogen through the sample, the change is not too abrupt, consistent with the data illustrated in Fig. 8.

Table 4: Experimental data from Alloy 1, used to plot Fig. 8. The hydrogen content listed is that evolved from the sample over the temperature range 25-300°C, using the heating rate indicated.

Number	V_γ	Charging time / h	$\dot{T}$/°C h^{-1}	Desorbed H / ppmw
1	0.07	24	100	1.78
2	0.07	24	100	1.45
3	0.10	24	100	1.01
4	0.15	24	100	1.19
5	0.21	24	100	1.25
6	0.21	24	50	0.84
7	0.21	24	75	1.02
8	0.21	20	100	0.89
9	0.21	20	100	1.00
10	0.21	1	100	0.02
11	0.21	3	100	0.14
12	0.21	6	100	0.33
13	0.07	1	100	0.08
14	0.07	3	100	0.20
15	0.07	6	100	0.24

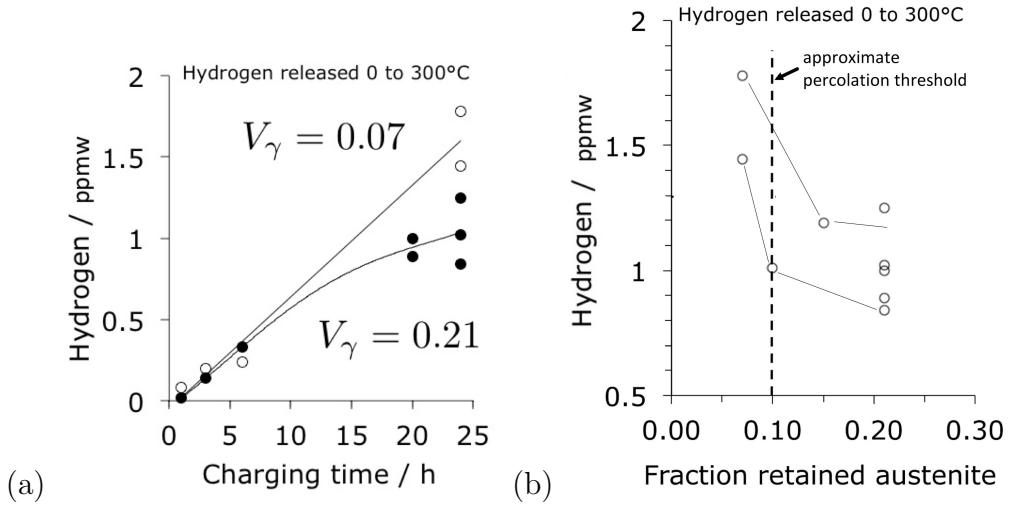

Figure 8: Alloy 1. (a) Dependence of hydrogen desorbed over the temperature range 25-300°C, on the hydrogen charging time, and b) on the volume fraction of retained austenite.

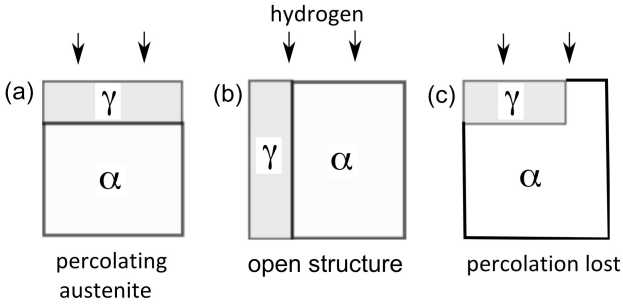

Figure 9: Different scenarios in a simplified model for the penetration of hydrogen into a two-phase mixture of ferrite and austenite.

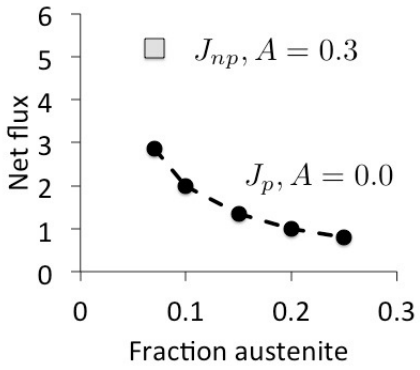

Figure 10: Calculated net flux, taking J_α has an arbitrary value equal to 15. Details in text.

4.5. Permeation experiments

The raw permeation data from experiments conducted on Alloy 2 samples heat-treated as described in Table 2 are presented in Fig. 11a. The derived effective-diffusivity data plotted in Fig. 11b confirm the general expectation that the presence of the films of retained austenite reduces the effective diffusivity of hydrogen through the sample very significantly, irrespective of the analysis method. The two methods give different answers because the time-lag method treats the problem essentially as a random walk of hydrogen through the steel, whereas the break-through technique equation is derived on the ability of the hydrogen to begin arriving on the other (output) side of the sample. The smaller value of the time-lag diffusivity $D_l < D_b$ indicates that the hydrogen transport is governed by diffusion through the sheet rather than by surface kinetics.

Permeability represents the ability of a material to act as a hydrogen barrier, determined from the steady state current through the sample. This

is in contrast to diffusivity, which describes the kinetics of atomic motion. The permeability increases dramatically as the retained austenite content is reduced and percolation is lost, as shown in Fig. 11.

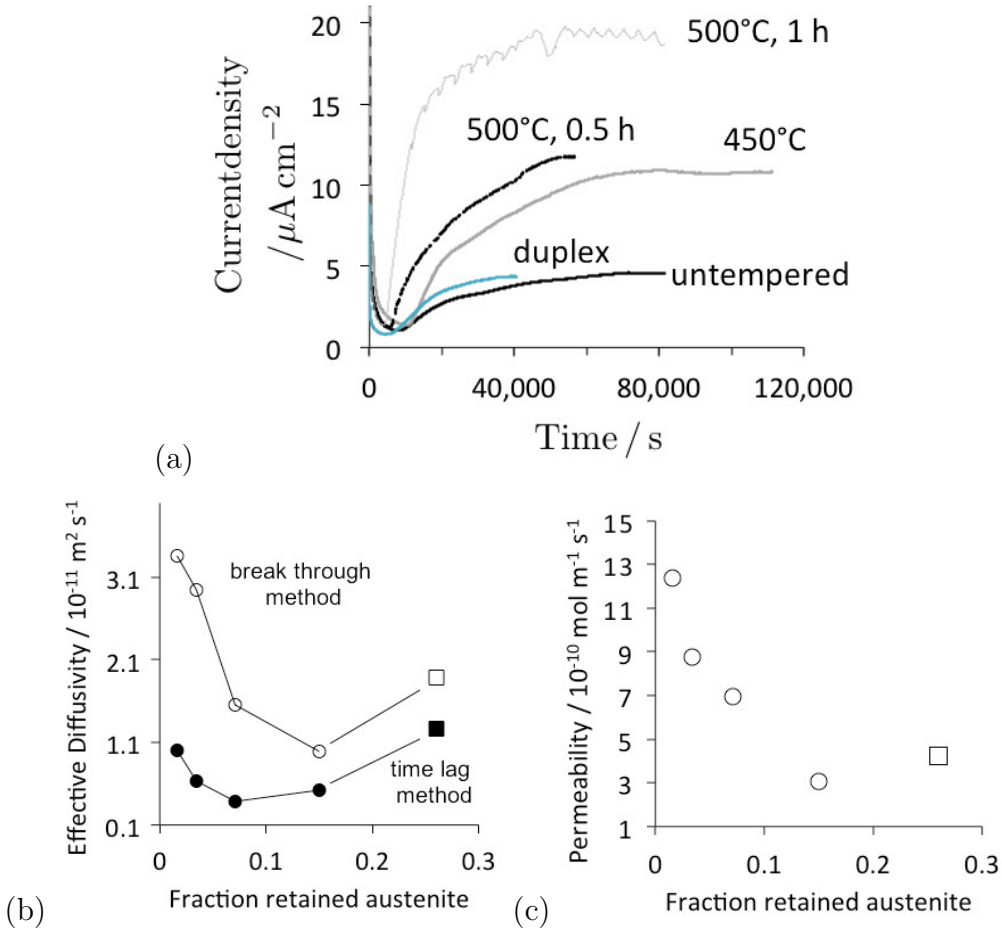

Figure 11: Permeation experiments on samples of Alloy 2 (circles) and the duplex steel (squares). (a) Current density versus time. (b) Effective diffusivities D_l and D_b. (c) permeability data.

In all of the TDA experiments on charged specimens, no significant hydrogen-desorption was observed in the temperature range 300–400°C.

4.6. Decomposition of retained austenite

It was also intended to study what happens to the hydrogen dissolved in the austenite, when the austenite associated with the bainitic structure decomposes into a mixture of cementite and ferrite. Previous work on nanostructured bainite has shown that the decomposition occurs during isothermal heat treatment at temperatures of 400°C or above [27, 29, 38, 39]. However, the present experiments involve continuous heating, so dilatometric experiments were done to measure the temperature range over which the substantive decomposition of austenite occurs. Given that the retained austenite is enriched in carbon to at least 1.2 wt% [40], its decomposition in the manner described was calculated to lead to a net contraction using the equations given in [41]. Fig. 12 shows that for both heating rates studied, the austenite decomposes in a temperature range of approximately 420-530°C.

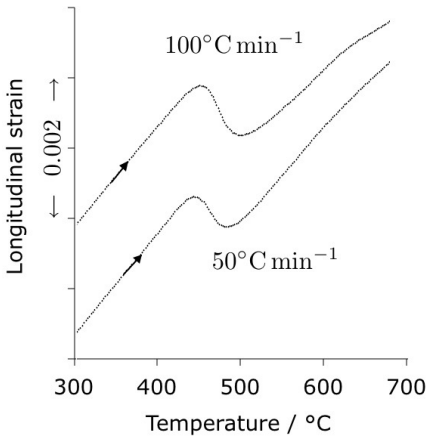

Figure 12: Alloy 1. Length changes during the heating of the $V_\gamma = 0.21$ sample. The contractions observed during heating correspond to the decomposition of the carbon-enriched retained austenite.

At the kind of heating rates used in the present work, even strongly trapped hydrogen (binding energy $\approx 50\,\mathrm{J\,mol^{-1}}$) should escape from the sample by the point where it reaches 300°C [33, 42]. Any hydrogen which is even more strongly trapped is unlikely to contribute to the deterioration of mechanical properties [43]. The TDA curves presented earlier show that much of the harmful hydrogen is removed by 300°C. However, to investigate whether the decomposition of austenite into a mixture of cementite and ferrite releases strongly trapped hydrogen, many of the experiments were continued to temperatures as high as 800°C.

Unfortunately, the experiments revealed rather strange results, both over

the temperature range of interest from the point of view of austenite decomposition, and beyond, Fig. 13. It was suspected that oxidation plays a role in creating these effects. The 99.9995% pure gas contains, according to the supplier, some 2 ppm of water. The thermodynamic analysis presented in Appendix A shows that with an assumed value of $p_{H_2}/p_{H_2O} = 0.1$ given the very low concentration of water in the gas, it is possible in all the steels studied here to reduce the water into hydrogen, with the formation of Si, Al and Mn oxides (Fig. 13b). FeO can also form but the driving force for oxidation is rather small so it is likely that the other oxides form preferentially.

To test this experimentally, a sample of the duplex steel was polished, charged and tested to generate a TDA curve, Fig. 13c. The same sample was then polished and reheated without hydrogen charging in the TDA, and on the third occasion, the same sample was reheated without charging or polishing in the TDA. The data indicate that the high-temperature effects are associated with oxidation, and that the presence of an existing oxide film tends to diminish the effect, as seen in the third experiment (Fig. 13c(iii)).

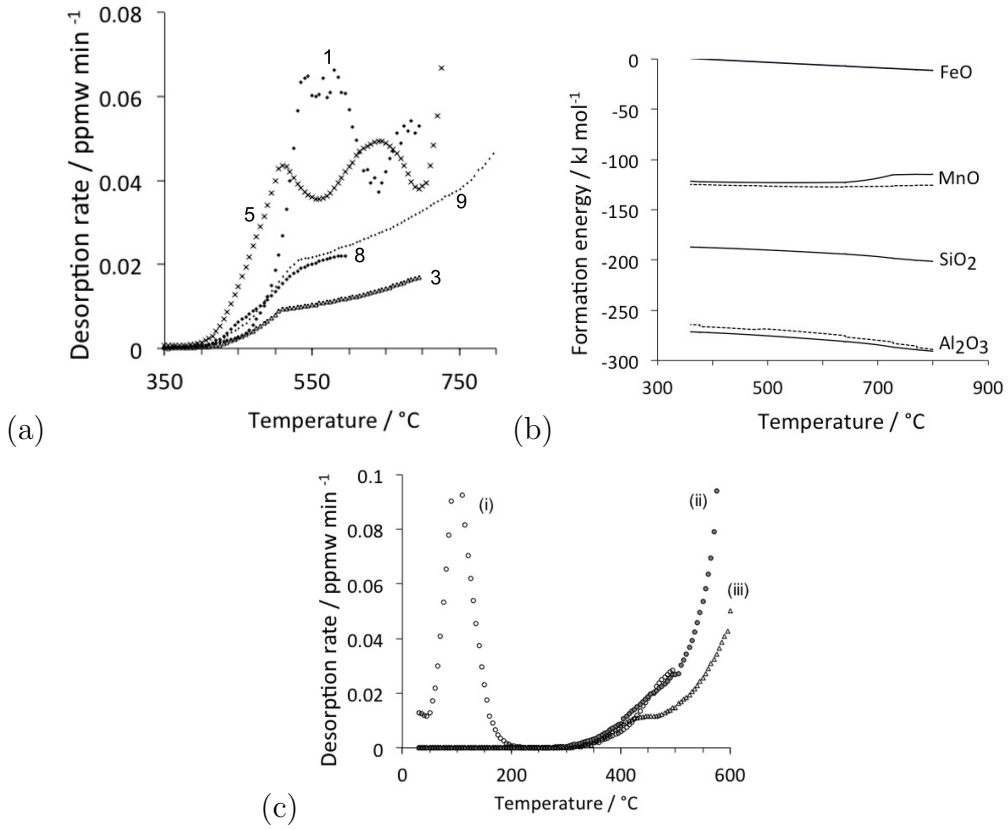

Figure 13: (a) TDA data for Alloy 1; the numbers relate to those in Table 4. (b) Calculated free energy change for oxidation, for Alloy 1 (continuous lines) and Alloy 3 (dashed lines). (c) Data for the duplex steel sample Alloy 3, 1 mm thick, hydrogen charged for 24 h, 100°C min^{-1}. (i) Polished, charged and analysed, (ii) same sample, polished and analysed without charging, (iii) same sample, not polished or charged, analysed.

5. Conclusions

The essential purpose of the work was to study the passage of hydrogen through a mixture of bainitic ferrite and films of austenite, in which the austenite fraction and morphology was such that it forms a continuous barrier between the ferrite plates, i.e., the austenite percolates through the mixture. The fraction of austenite could be controlled by heat treatment so that corresponding samples where the fraction is less than that required for percolation could be studied. The following conclusions can be reached on the basis of thermal desorption experiments, permeation experiments, theoretical analysis and comparison between samples containing radically different morphologies of austenite at approximately the same volume fraction:

1. The study of partially hydrogen-charged specimens of nanostructured bainite using thermal desorption shows that the amount of hydrogen absorbed by the steel, at long charging times, is smaller when the austenite fraction is beyond the percolation threshold. Indeed, the amount of hydrogen that enters the steel increases sharply when the fraction of austenite is less than the percolation threshold.
2. In the nanostructured steel, the quantity of hydrogen that enters the steel during charging is not as sensitive to the austenite content as might be expected from a raw comparison of the diffusion coefficients of hydrogen in ferrite. This is because the diffusivity of hydrogen in bainitic ferrite is in fact much smaller than that for 'perfect' ferrite, due to trapping effects.
3. Consistent with experimental data, a simple flux model indicates that the increase in the hydrogen absorbed by the steel during charging is about a factor of two when the austenite in the nanostructure loses percolation.
4. A comparison of two steels, one with the percolating austenite films ($V_\gamma = 0.15$) in the nanostructure, and the other where the fraction of austenite is much larger ($V_\gamma = 0.26$) but where the austenite grains are present in a continuous ferrite matrix, indicates a very strong effect of austenite morphology on the penetration of hydrogen into the steel. The latter microstructure much more readily absorbs the hydrogen.

In summary, the nanostructured bainite containing percolating austenite should resist the influx of hydrogen better than in the absence of austenite, but the resistance vanishes if the austenite is present as isolated grains in

a predominantly ferritic structure. The work also verifies the calculation [8] that the percolation threshold in such bainite is at approximately $V_\gamma \approx 0.1$, a factor important in controlling the ductility of the steel.

Acknowledgments: The authors are grateful to the Worshipful Company of Ironmongers, Tata Steel UK, the EPSRC, to the World Class University Programme of the National Research Foundation of Korea, Ministry of Education, Science and Technology, project number R32–2008–000–10147–0, and the POSCO Steel Innovation Programme for supporting this work; to Dr Hala Salman Hasan for assistance with sample preparation; to Dr Giulio Lampronti for assistance with X-ray analysis.

All the data obtained during the course of this work have been made freely available on the web at the following address: http://www.msm.cam.ac.uk/phase-trans/2014/hydrogen.zip

Appendix A. Thermodynamics of oxidation

Assuming the manufacturer's statement that the the gas used in the thermal desorption analysis contains about 2 ppm of water, and that the evolved hydrogen is typically one tenth of this value at any instant of time, the ratio of partial pressures $p_{\mathrm{H_2}}/p_{\mathrm{H_2O}} \approx 0.1$, the oxidation of elements within the steel may be represented by the following equation:

$$\begin{aligned} \mathrm{H_2O} + \frac{x}{y}\mathrm{Me} &= \frac{1}{y}\mathrm{Me}_x\mathrm{O}_y + \mathrm{H_2} \\ \Delta G &= \Delta G^\circ_{\mathrm{Me}_x\mathrm{O}_y} - \Delta G^\circ_{\mathrm{H_2O}} + RT \ln \frac{a^{\frac{1}{y}}_{\mathrm{Me}_x\mathrm{O}_y} p_{\mathrm{H_2}}}{p_{\mathrm{H_2O}} a^{\frac{x}{y}}_{\mathrm{Me}}} \end{aligned} \qquad \text{(A.1)}$$

where 'Me' represents the metal, x and y depend on the type of oxide as listed in Table A.5, a represents the activity of the material identified by the subscript, and R is the gas constant. The activity of the pure oxide was always taken to be unity, and those of the metallic elements in the steel concerned calculated using ThermoCalc [44].

Table A.5: Thermodynamic data for oxidation

Reaction	Standard free energy change / kJ mol^{-1}	Reference
$H_2 + \frac{1}{2}O_2 = H_2O$	$\Delta G^\circ_{H_2O} = -247.70 + 0.0558T$	[45]
$Fe + \frac{1}{2}O_2 = FeO$	$\Delta G^\circ_{FeO} = -264.00 + 0.0646T$	[45]
$Mn + \frac{1}{2}O_2 = MnO$	$\Delta G^\circ_{MnO} = -388.90 + 0.0763T$	[46]
$\frac{1}{2}Si + \frac{1}{2}O_2 = \frac{1}{2}SiO_2$	$\Delta G^\circ_{SiO_2} = -473.15 + 0.0988T$	[45]
$\frac{2}{3}Al + \frac{1}{2}O_2 = \frac{1}{3}Al_2O_3$	$\Delta G^\circ_{Al_2O_3} = -561.00 + 0.1077T$	[45]

References

[1] F. G. Caballero, H. K. D. H. Bhadeshia, K. J. A. Mawella, D. G. Jones, and P. Brown. Design of novel high–strength bainitic steels: Part I. *Mater. Sci. Technol.*, 17:512–516, 2001.

[2] F. G. Caballero, H. K. D. H. Bhadeshia, K. J. A. Mawella, D. G. Jones, and P. Brown. Design of novel high–strength bainitic steels: Part II. *Mater. Sci. Technol.*, 17:517–522, 2001.

[3] C. Garcia-Mateo and F. G. Caballero. Role of retained austenite on tensile properties of steels with bainitic microstructures. *Mater. Trans.*, 46:1839–1846, 2005.

[4] H. K. D. H. Bhadeshia. The first bulk nanostructured metal. *Sci. Technol. Adv. Mater.*, 14:014202, 2013.

[5] C. Garcia-Mateo, F. G. Caballero, and H. K. D. H. Bhadeshia. Mechanical properties of low–temperature bainite. *Mater. Sci. Forum*, 500–501:495–502, 2005.

[6] C. Garcia-Mateo and F. G. Caballero. Ultrahigh–strength bainitic steels. *ISIJ Int*, 45:1736–1740, 2005.

[7] C. Garcia-Mateo, F. G. Caballero, T. Sourmail, M. Kuntz, J. Cornide, V. Smanio, and E. Elvira. Tensile behaviour of a nanocrystalline bainitic steel containing 3 wt*Mater Sci Eng A*, 549:185–192, 2012.

[8] H. K. D. H. Bhadeshia. Nanostructured bainite. *Proc. Roy. Soc. A*, 466:3–18, 2010.

[9] H. K. D. H. Bhadeshia and D. V. Edmonds. Bainite in silicon steels: a new composition property approach i. *Met. Sci.*, 17:411–419, 1983.

[10] B. P. J. Sandvik and H. P. Nevalainen. Structure-property relationships in commercial low-alloy bainitic-austenitic steel with high strength, ductility, and toughness. *Met. Technol.*, 8:213–220, 1981.

[11] J. R. Patel and M. Cohen. Criterion for the action of applied stress in the martensitic transformation. *Acta. Metall.*, 1:531–538, 1953.

[12] N.K. Balliger and T. Gladman. Work hardening of dual-phase steels. *Met. Sci.*, 15:95–108, March 1981.

[13] C. A. N. Lanzillotto and F. B. Pickering. Structure-property relationships in dual-phase steel. *Met. Sci.*, 16:371–382, 1982.

[14] K. Hase, C. Garcia-Mateo, and H. K. D. H. Bhadeshia. Bimodal size–distribution of bainite plates. *Mater Sci Eng A*, A438–440:145–148, 2006.

[15] M. Y. Sherif. *Characterisation and development of nanostructured, ultrahigh strength, and ductile bainitic steels*. University of Cambridge, 2005.

[16] G. B. Olson and M. Cohen. Kinetics of strain–induced martensitic transformation. *Metall Trans A.*, 6A:791–795, 1975.

[17] K. Sugimoto, N. Usui, M. Kobayashi, and S. Hashimoto. Effects of volume fraction and stability of retained austenite on ductility of TRIP–aided dual–phase steels. *ISIJ Int*, 32:1311–1318, 1992.

[18] M. Sherif, C. Garcia-Mateo, T. Sourmail, and H. K. D. H. Bhadeshia. Stability of retained austenite in TRIP–assisted steels. *Mater. Sci. Technol.*, 20:319–322, 2004.

[19] H. K. D. H. Bhadeshia. Properties of fine–grained steels generated by displacive transformation. *Mater Sci Eng A*, 481–482:36–39, 2008.

[20] P. J. Jacques, E. Girault, Ph. Harlet, and F. Delannay. Developments of cold-rolled TRIP-assisted multiphase steels. low silicon TRIP-assisted multiphase steels. *ISIJ Int*, 41:1061–1067, 2001.

[21] W. Y. Choo and J. Y. Lee. Thermal analysis of trapped hydrogen in pure iron. *Metall Trans A.*, 13:135–140, 1982.

[22] K. Ono and M. Meshii. Hydrogen detrapping from grain boundaries and dislocations in high purity iron. *Acta. Metall. Mater.*, 40:1357–1364, 1992.

[23] F. G. Caballero, H. K. D. H. Bhadeshia, K. J. A. Mawella, D. G. Jones, and P. Brown. Very strong, low–temperature bainite. *Mater. Sci. Technol.*, 18:279–284, 2002.

[24] C. Garcia-Mateo, F. G. Caballero, and H. K. D. H. Bhadeshia. Acceleration of low–temperature bainite. *ISIJ Int*, 43:1821–1825, 2003.

[25] D. J. Dyson and B. Holmes. Effect of alloying additions on the lattice parameter austenite. *J. Iron Steel Inst.*, 208:469–474, 1970.

[26] D. K. Han. Hydrogen assisted cracking of ferritic linepipe steel and corrosion behaviour of austenitic twip steel. Master's thesis, Pohang University of Science and Technology, Pohang, Republic of Korea, 2013.

[27] C. Garcia-Mateo, M. Peet, F. G. Caballero, and H. K. D. H. Bhadeshia. Tempering of a hard mixture of bainitic ferrite and austenite. *Mater. Sci. Technol.*, 20:814–818, 2004.

[28] M. Peet. *Transformation and tempering of low–temperature bainite*. PhD thesis, University of Cambridge, Cambridge, U. K., 2010.

[29] H. S. Hasan, M. J. Peet, and H. K. D. H. Bhadeshia. Severe tempering of bainite generated at low transformation temperatures. *Int. J Mater. Research*, 103:1319–1324, 2012.

[30] L. S. Darken. Diffusion of carbon in austenite with a discontinuity of composition. *Trans. AIME*, 180:430–438, 1949.

[31] J. P. Hirth. Effects of hydrogen on the properties of iron and steel. *Metall. Mater. Trans. A*, 11(861–890), 1980.

[32] Y. D. Park, I. S. Maroef, A. Landau, and D. L. Olson. Retained austenite as a hydrogen trap in steel welds. *Weld. J., Research Supplement*, 81:27S–35S, 2002.

[33] E. J. Song, D. W. Suh, and H. K. D. H. Bhadeshia. Theory for hydrogen desorption in ferritic steel. *Comp. Mater. Sci.*, 79:36–44, 2013.

[34] X. Sun, J. Xu, and Y. Li. Hydrogen permeation behaviour in austenitic stainless steels. *Mater Sci Eng A*, 114:179–187, 1989.

[35] B. D. Craig. On the elastic interaction of hydrogen with precipitates in lath martensite. *Acta Metall.*, 25:1027–1030, 1977.

[36] N. Yurioka and H. Suzuki. Hydrogen-assisted cracking in C-Mn and low alloy steel weldments. *Int Mater Rev*, 35:217–249, 1990.

[37] A. Turnbull and R. B. Hutchings. Analysis of hydrogen diffusion in a two-phase alloy. *Mater Sci Eng A*, 177:161–171, 1994.

[38] F. G. Caballero, M. K. Miller, and C. Garcia-Mateo. Atom probe tomography analysis of precipitation during tempering of a nanostructured bainitic steel. *Metall. Mater. Trans. A*, 42:3660–3668, 2011.

[39] C. N. Hulme-Smith, I. Lonardelli, M. J. Peet, A. C. Dippel, and H. K. D. H. Bhadeshia. Enhanced thermal stability in nanostructured bainitic steel. *Scripta Mater*, 69:191–194, 2013.

[40] F. G. Caballero, C. García-Mateo, M. J. Santofimia, M. K. Miller, and C. Garcia de Andrés. New experimental evidence on the incomplete transformation phenomenon in steel. *Acta Mater*, 57:8–17, 2009.

[41] A. Saha Podder and H. K. D. H. Bhadeshia. Thermal stability of austenite retained in bainitic steels. *Mater Sci Eng A*, 527:2121–2128, 2010.

[42] J. H. Ryu, Y. S. Chun, C. S. Lee, H. K. D. H. Bhadeshia, and D. W. Suh. Effect of deformation on hydrogen trapping and effusion in TRIP-assisted steel. *Acta Mater*, 60:4085–4092, 2012.

[43] K. Takai and R. Watanuki. Hydrogen in trapping states innocuous to environmental degradation of high-strength steels. *ISIJ Int*, 43:520–526, 2003.

[44] J. O. Andersson, T. Helande, L. Hoglund, P. Shi, and B. Sundman. Thermo-Calc & DICTRA, computational tools for materials science. *CALPHAD*, 26:273–312, 2002.

[45] D. R. Stull and H. Prophet. JANAF thermochemical tables. Technical Report NSRDS-NBS-37, National Bureau of Standards, Washington, D. C., USA, 1971.

[46] E. T. Turkdogan. *Physical Chemistry of High Temperature Technology*, volume 5. Academic Press, New York, USA, 1980.

List of Figure Captions

Figure 1: Schematic diagrams showing (a) thermal desorption and (b) Devanathan-Stachurski permeation cell used.

Figure 2: Alloy 1. (a) As-transformed structure, with the darker regions representing retained austenite. (b) Structure containing some carbide particles, after tempering 450°C for 2 h. (c) After tempering 500°C for 0.5 h. (d) After tempering 500°C for 1 h. Carbide particles are arrowed.

Figure 3: Alloy 2. (a) As-transformed structure, with the darker regions representing retained austenite. (b) After tempering 450°C for 2 h. (c) After tempering 500°C for 0.5 h. (d) After tempering 500°C for 1 h. Carbide particles are arrowed.

Figure 4: Electron diffraction patterns confirming the presence of cementite. (a) Alloy 1, after tempering at 450°C for 2 h. (b) Alloy 1, after tempering at 500°C for 1 h. (c) Alloy 2, after tempering at 500°C for 30 min. (d) Alloy 2, after tempering at 500°C for 1 h.

Figure 5: Alloy 3. EBSD phase map with red and white regions indicating austenite ($V_\gamma = 0.26$) and ferrite respectively.

Figure 6: Thermal desorption analysis experiments at $100°C\,min^{-1}$, $V_\gamma = 0.21$. (a) Alloy 1, behaviour of an uncharged specimen. (b) Alloy 1, samples charged with hydrogen for 20 h. The two curves are from two physically different samples, identically produced before the TDA. (c) Comparison between TDA curves of 4 mm thick Alloy 1 samples, and 1 mm thick Alloy 2 sample.

Figure 7: Alloy 1. TDA data collected after charging each of specimen with hydrogen for 24 h, using a heating rate of $100°C\,min^{-1}$. The continuous line, triangles and circles correspond to $V_\gamma = 0.21$, 0.15, 0.10 of retained austenite. The dashed curves are for $V_\gamma = 0.07$, although one of these is not easily distinguished on the diagram, but lies between the triangles and circles.

Figure 8: Alloy 1. (a) Dependence of hydrogen desorbed over the temperature range 25-300°C, on the hydrogen charging time, and b) on the volume

fraction of retained austenite.

Figure 9: Different scenarios in a simplified model for the penetration of hydrogen into a two-phase mixture of ferrite and austenite.

Figure 10: Calculated net flux, taking J_α has an arbitrary value equal to 15. Details in text.

Figure 11: Permeation experiments on samples of Alloy 2 (circles) and the duplex steel (squares). (a) Current density versus time. (b) Effective diffusivities D_l and D_b. (c) permeability data.

Figure 12: Alloy 1. Length changes during the heating of the $V_\gamma = 0.21$ sample. The contractions observed during heating correspond to the decomposition of the carbon-enriched retained austenite.

Figure 13: (a) TDA data for Alloy 1; the numbers relate to those in Table 4. (b) Calculated free energy change for oxidation, for Alloy 1 (continuous lines) and Alloy 3 (dashed lines). (c) Data for the duplex steel sample Alloy 3, 1 mm thick, hydrogen charged for 24 h, $100^\circ\mathrm{C\,min^{-1}}$. (i) Polished, charged and analysed, (ii) same sample, polished and analysed without charging, (iii) same sample, not polished or charged, analysed.